Alternative Method of the Thermospheric Atomic Oxygen Density Determination

Adam C. Bennett[a] and Kazem Omidvar[b]

[a]Physics Department, Taylor University, Upland, IN
[b]Data Assimilation Office, NASA/Goddard Space Flight Center, Greenbelt, MD

August 10, 2000

Abstract Atomic oxygen density in the upper thermosphere (~300 km) can be calculated using ground based incoherent scatter radar and Fabry-Perot interferometer measurements. Burnside et al. [1991] was the first to try this method, but Buonsanto et al. provided an extensive treatment of the method in 1997. This paper further examines the method using 46 nights of data collected over six years and the latest information on the oxygen collision frequency. The method is compared with the MSIS-86 atomic oxygen prediction values, which are based upon *in situ* rocket born and satellite measurements from the 70's to the mid-80's. In general, the method supports the MSIS-86 model, but indicates several areas of discrepancy. Furthermore, no direct correlation is found between the geomagnetic conditions and the difference between the method and MSIS-86 predictions.

Introduction

Due to its extreme height, elusiveness has often pervaded study of the thermosphere. In this respect, measurement of neutral atomic oxygen density ([O]) has been no different. Because of the lack of a constant data supply, researchers have had to rely upon the MSIS-86 model for calculations requiring thermospheric oxygen densities. While Hedin's model has proven to be generally reliable, it has limits and significant error margins. As indicated by Hedin [1987] and Grossmann et al. [2000], MSIS predictions below 200 km become increasingly divergent from reality due to the lack of data for this region. Grossmann's results from the CRISTA experiments indicated an average of 40% less [O] than predicted during low solar activity. Buonsanto et al. [1997] estimated a 20% uncertainty for MSIS predictions higher in the thermosphere based on the information in Hedin [1987]. Burnside et al. [1991] found large errors during geomagnetically disturbed periods above Arecibo at 300 km with measured densities twice the predictions.

Such uncertainties for [O] predictions are unsatisfactory because atomic oxygen plays an important role in various thermospheric reactions. At an altitude of 120 km, neutral atomic oxygen constitutes roughly 20% of the total density of the atmosphere. Here it affects the heat transfer between the mesosphere and lower thermosphere by recombining into O_2 and deactivating CO_2 [Ward et al., 1993]. At an altitude of 300 km, neutral atomic oxygen constitutes roughly 80% of the total density of the atmosphere. Here it moves solar energy deeper into earth's thermosphere by transferring an electron through strong resonance charge exchange interaction with O^-, providing the principal method of heating the thermosphere [Omidvar et al., 1998].

Within the last decade, several methods have been introduced to calculate neutral atomic oxygen density for various areas of the thermosphere, including twilight 7320 Å airglow

emissions [McDade et al., 1991], satellite far ultraviolet images (DE 2) [Drob et al., 1999], satellite 63 μm infrared measurements (CRISTA) [Grossmann et al., 2000], and a host of rocket born measurements for the 80 to 200 km range [partial list: Shepherd et al., 1995; Kita et al., 1996; Melo et al., 1996]. A new technique for determining [O] at about 300 km using ground based incoherent scatter radar (ISR) and Fabry-Perot interferometer (FPI) measurements was introduced at the beginning of the decade. Burnside et al. [1991] was the first to use this technique, which he applied to data collected at Arecibo. Buonsanto et al. [1992] provided a fuller treatment of the technique at Millstone Hill for fourteen nights of data ranging from March 19, 1990 to May 16, 1991. In this paper, we will further examine this technique for 46 nights with a larger data set, a greater span of time, and the most recent information on O^+-O collision frequency.

Data Collection and Instrumentation

The data selected provides a wide spectrum of solar and geomagnetic activity. The data set includes 46 nights and 899 points of coincident ISR and FPI measurements from Aug. 19, 1988 to Mar. 3, 1995 at Millstone Hill Observatory in Massachusetts, USA (42.6° N and 71.5° W). Table 1 lists every night of collected data. Buonsanto et al. [1997] originally processed the data.

By employing Thomson backscatter from ionospheric electrons, the incoherent scatter radar (ISR) is able to ascertain ion velocity along the magnetic field ($V_{\|}$), ion (electron) density (N_i), ion temperature (T_i), and electron temperature (T_e). The Fabry-Perot interferometer (FPI) observes the atomic oxygen at 630 nm and calculates the neutral wind velocity (U) by reading the Doppler shift of the nightglow. Although the FPI can also provide neutral temperature measurements, these tend to have large uncertainties, making them less reliable than the radar measurements. The ISR is able to operate nearly continuously, but poor visibility from cloudy nights limits data from the FPI.

By combining the ISR electron density profile with data from the MSIS-86 model, the altitude of the maximum 630 nm emissions was estimated for each data point [Link & Cogger, 1988]. It is at this altitude that the FPI makes its neutral wind velocity (U) readings, so all ISR data was selected for this altitude. Furthermore, the MSIS-86 atomic oxygen density predictions were also based upon this altitude. The maximum emission altitude tends to range about 50 km on any one night and may be as low as 250 km or as high as 350 km. It is generally about 300 km.

For more information on the data collection and instrumentation, we recommend Sipler et al. [1991] and Buonsanto et al. [1997]. Sipler provides a complete discussion of the FPI and a summary of the ISR, and both Sipler and Buonsanto nicely overview the data collection for substantial portions of the same data used in this study.

Theory: From Diffusion Velocity to Oxygen Density

The diffusion velocity of the ions (V_d) can be calculated through two different forms:

$$V_d = U\cos I - V_{\|} \tag{1}$$

$$V_d = -\frac{2kT_p}{m_i \nu_{in}}\left[\frac{1}{N_i}\frac{\partial N_i}{\partial z} + \frac{1}{T_p}\frac{\partial T_p}{\partial z} + \frac{m_i g}{2kT_p}\right]\sin I \tag{2}$$

where $T_p = (T_i + T_e) / 2$ is the plasma temperature, U the horizontal meridional neutral wind velocity, I the magnetic dip angle, $V_{||}$ the ion velocity along the magnetic field, k the Boltzmann constant, m_i the ion mass, ν_{in} the ion-neutral collision frequency, N_i the ion (electron) density, z the altitude, and g the acceleration due to gravity [Reddy et al., 1994]. It is assumed that the ionosphere is composed of O^+, so all calculations refer to this ion.

The collision frequency is an important component of Equation (2). At 300 km, the main contributions to ν_{in} are O^+-O, O^+-N_2, and O^+-O_2 collisions, of which the O^+-O collision frequency is the largest because of the high concentration of neutral atomic oxygen. Due to the difficult nature of experimentally determining ν_{in} at low energies, we must use a theoretical formula instead:

$$\nu_{in}^{th} = \nu_{O^+-O}^{th} + \nu_{O^+-N_2} + \nu_{O^+-O_2} , \tag{3}$$

$$\nu_{in}^{th} = Q_d^{th}[O] + 6.9\times10^{-16}[N_2] + 6.7\times10^{-16}[O] , \tag{4}$$

where Q_d is the theoretical collision cross section of O^+-O. Because N_2 and O_2 are minor constituents of the thermosphere at 300 km (roughly 19% and 1%), their collision frequencies are approximated using Banks [1996] and MSIS-86 density predictions without appreciable inaccuracies.

Conversely, the ν_{O+-O} has a large impact on the results. Its exact value has been the topic of much research and debate, especially over the last decade. For a considerable time, theoretical results varied significantly, but the recent correlation in the formulas by Stubbe [1968], Stallcop et al. [1991], and Pesnell et al. [1993], has provided a firmer foundation. The formula by Pesnell et al. is given by:

$$Q_d^{th} = 3.0\times10^{-17} T_r^{1/2}\left(1 - 0.135\log T_3\right)^2 \tag{5}$$

where $T_r = (T_i + T_n) / 2$, with T_n the neutral temperature and $T_3 = T_r / 1000$. Pesnell's formula is larger than the commonly used formula of Dalgarno [1964] by 1.38, 1.32, 1.28, 1.24, and 1.22 at 500 K, 750 K, 1000 K, 1250 K, and 1500 K respectively.

The quest for empirical verification of Q_d started roughly, but has began to come into focus. Burnside et al. [1987] used ISR and FPI data from Arecibo to calculate ν_{O+-O}, but his values were 1.7 times larger than those predicted by Dalgarno. Sipler et al. [1991] used a similar technique at Millstone Hill to calculate values 1.9 times larger than Dalgarno, and Salah [1993] recommended an official correction value of F = 1.7, which was termed the Burnside Factor.

In the next few years, a series of papers found fault with the previous data analysis methods. Reddy et al. [1994] demonstrated a systematic overestimate of Q_d from errors in the measurements. Hines et al. [1997] questioned the use of the least-squares method in this application. Buonsanto et al. [1997] conducted Monte Carlo simulations on Millstone Hill data, discovered a systematic overestimate from random errors, and calculated an unbiased $F \approx 1.4\pm0.3$. Finally, Omidvar et al. [1998] conducted three different analysis methods on the Millstone Hill data and determined it supported the theoretical formula by Pesnell et al.

If the collision frequency is now assumed to be known, we can determine neutral atomic oxygen density in the thermosphere using Equations (1) and (2) as follows:

$$V_d = U\cos I - V_{||} = W\,, \tag{6}$$

$$V_d = \frac{-\frac{2kT_p}{m_i}\left[\frac{1}{N_i}\frac{\partial N_i}{\partial z} + \frac{1}{T_p}\frac{\partial T_p}{\partial z} + \frac{m_i g}{2kT_p}\right]\sin I}{Q_d^{th}[O] + 6.9\times10^{-16}[N_2] + 6.7\times10^{-16}[O_2]}\,. \tag{7}$$

We introduce

$$\gamma = -\frac{2kT_p}{m_i}\left[\frac{1}{N_i}\frac{\partial N_i}{\partial z} + \frac{1}{T_p}\frac{\partial T_p}{\partial z} + \frac{m_i g}{2kT_p}\right]\sin I \tag{8}$$

and

$$\nu_{correction} = 6.9\times10^{-16}[N_2] + 6.7\times10^{-16}[O_2]\,. \tag{9}$$

Then Equations (6) and (9) imply

$$O = \frac{D}{W} \tag{10}$$

where

$$D = \frac{\gamma - W\nu_{correction}}{Q_d^{th}}\,, \tag{11}$$

O is the neutral atomic oxygen density, γ groups many of the terms from Equation (2), $\nu_{correction}$ accounts for the $\nu_{O+\text{-}N2}$ and $\nu_{O+\text{-}O2}$, W is the diffusion velocity from both ISR and FPI wind data, and D is the theoretical portion from ISR temperature data.

Analysis

The past two studies of atomic oxygen density by Burnside et al. [1991] and Buonsanto et al. [1992] used a correction factor F = 1.7 and Dalgarno's formula for Q_d. Based upon Omidvar et al. [1998], the present work uses a correction of F = 1.0 and Pesnell's formula for Q_d. We have adjusted all of Buonsanto's data accordingly.

To provide a method of evaluating the data with itself, we divide the original 899 points into two data sets: Set A from August 19, 1988 to March 23, 1990 with 445 points and Set B from March 29, 1990 to March 3, 1995 with 454 points. After removing all outliers that produce F values below 0.35 or above 3.0, Group A has 398 points and Group B has 390 points. Each point consists of a D, W, and O. The D and W are derived from empirical data, while the O is the MSIS-86 [O] prediction for the particular time, position, and altitude of the matching data.

In a perfect world, the MSIS derived [O] will equal the D/W derived [O], so we compare these two values to check the accuracy of using ISR-FPI data to measure [O], check the validity of the MSIS model, and check the accuracy of the theoretical value of Q_d. All comparison is conducted at the 5% level of significance.

The standard deviations for both data Sets A and B (Table 2) demonstrate their wide data spreads (see Figure 1 and 2). Both data sets are comparable. As can be seen in Figures 3 and 4, the D/W's from Set A and Set B are heavily skewed toward the right side, approximating a lognormal distribution. In order to perform correlation analysis upon the data, which requires a Gaussian distribution, we take the log of all the D/W data points. This transforms the data from an approximate lognormal distribution to an approximate Gaussian distribution (see Figures 5 and 6). The MSIS-86 O predictions already form Gaussian distributions.

The correlation analysis comparing O with D/W returned $r^2 = 0.237$ and $r^2 = 0.139$ for Set A and Set B respectively, indicating a low, but significant, association in their variances. In general, though, D/W does not follow the trends of O. The correlation coefficients produced from each night of data range from $r = 0.93$ to $r = -0.80$. Ten nights display a significant positive correlation. One night displayed a significant negative correlation. Twenty-four nights have no significant correlation. The remaining ten nights have less than six data points, so we did not calculate their individual correlation values.

Although O and D/W are of similar magnitudes, many data points have substantial differences. In Set A, D/W is at least ±25% greater than O for 217 points. In Set B, D/W is at least ±25% greater than O for 148 points.

Perhaps the best analysis of the data is on a night by night basis. Twenty-four nights have average percent differences of the absolute value between D/W and O greater than 40%. Nonetheless, data from eight nights closely follows MSIS predictions. One of the best examples is September 12, 1991, which has an average difference of 21.2% and a significant correlation of $r = 0.503$ (Figure 7).

For the majority of the nights, the data roughly approximates the MSIS-86 predictions but includes large deviations. On a few of these nights, the data is extremely erratic, with December 29, 1989 being one of the worst examples (Figure 8). The erratic nature of the density on this night results from both dramatic shifts in wind speed and large changes in D. A number of nights have consistently different trends from the MSIS-86 predictions, such as in Figures 9, 10, 11, and 12.

We found no significant positive correlation between the geomagnetic activity and the average percent difference between D/W and O (Figure 13). For example, April 10, 1990 exhibits increased densities during a geomagnetic storm reaching a max Kp of 8- (Figure 14), but so does January 26, 1995 even though it maintains a low Kp of 1 (Figure 15). This is somewhat in contrast to Burnside [1991] who suggested densities dramatically increased over MSIS-86 predictions during geomagnetically disturbed periods based upon measurements on July 14, 1985 (max Kp 4+) and January 15, 1988 (max Kp 7+).

Over half of the data was collected from Aug. 19, 1988 to September 21, 1990. This concentration of twenty-six nights over two years allows the opportunity to search for seasonal trends. We average each night of data to approximate the atomic oxygen density for that period of the year. Figure 16 shows a clear seasonal cycle with a winter maximum and summer minimum. In general, the alternative method produced averages larger than the MSIS-86 predicted averages.

Sources of Error

Error in the measurements of the two wind velocities (ion velocity from the ISR and the neutral wind velocity from the FPI) will have the largest effect upon the results. Both of these velocities factor into the calculation of the diffusion velocity (W). Buonsanto [1997] states that both items have error bars as much as 20%. Furthermore, he states that these random errors will skew data to the right when W is in denominator, as seen in Figures 3 and 4. This could tend to inflate our oxygen density values when errors are large.

Error in $V_{||}$ will increase if vertical winds are present because all measurements assume zero vertical winds. A study by Sipler et al. [1995] on nighttime vertical winds above Millstone Hill revealed downward movement on the order of 10 m/s with little variability on geomagnetically quiet nights (Kp≤3) and downward movement on the order of 0 to 50 m/s with great variability on geomagnetically active nights (Kp>3), but these values were difficult to determine because of error bars ranging from 10 up to 50 m/s. Sipler et al. also noted oscillations in the magnitude and direction of the vertical wind velocities. Unfortunately, we know little about such oscillations and our data set for this study does not include vertical wind information.

Vertical winds add an additional term to Equation (6) as such:

$$V_d = U\cos I + U_z \sin I - V_{||} = W \qquad (12)$$

where U_z is the vertical wind velocity. U_z will increase our oxygen density calculations because it tends to be negative. This error becomes especially significant during geomagnetically disturbed periods, when vertical winds may be large and highly variable. We must also consider the possible oscillatory nature of the winds when examining the data.

To determine if any systematic errors, such as listed above, are present in the data, we analyze Data Set A and B using the bias formula

$$bias = \frac{\sum_i (O_i - D_i/W_i)}{n \times \bar{O}} \qquad (13)$$

where O is the mean of the MSIS-86 oxygen predictions and n is the number of data points. The results are listed Table 2. These indicate a small systematic effect, but the majority of the errors are random.

Conclusion

This examination of ISR and FPI data provides three significant results:

1. The data generally supports the MSIS-86 model, although our method displays more detail and greater complexity than the MSIS-86 model predicts. Caution should be used, for this method also has the possibility for large errors under certain conditions.

2. A number of nights exhibited trends that were consistently different from MSIS-86 predictions. These nights indicate needed refinement in the MSIS-86 model.

3. Geomagnetic activity does not appear to have a simple one-to-one impact upon the average difference between MSIS-86 predictions and the alternative method. Much of the impact is disguised either by random errors or the competition between horizontal and vertical wind velocities in the end results.

In conclusion, employing ISR and FPI data to calculate atomic oxygen density in the higher thermosphere provides a ground based method to monitor changes. Unfortunately, the method requires simultaneous measurements from large and unique equipment that is available at only a few locations in the world. Furthermore, the FPI requires a clear sky. Although limited by these factors, this method has the benefit of allowing detailed, long-term study of upper thermosphere atomic oxygen density.

Acknowledgements

This research was conducted under the 2000 Undergraduate Summer Institute on Atmospheric and Hydrospheric Sciences program at the NASA/Goddard Space Flight Center. Foremost, the authors thank the late Dr. Buonsanto who provided the original data from Haystack Observatory at Millstone Hill, operated by the Massachusetts Institute of Technology. Although he had a short life, he was very productive in his research. His presence is missed. Additionally, the authors thank Dr. Sipler at Haystack Observatory for personal correspondence concerning the data, the National Space Science Data Center for Kp values, and the World Data Center of Solar-Terrestrial Physics for MSIS-86 calculations.

References

Banks, Peter, Collision frequencies and energy transfer: Ions, *Planet. Space Sci.*, **14**, 1105-1122, (1966).

Buonsanto, M. J., D. P. Sipler, G. B. Davenport, and J. M. Holt, Estimation of the O+, O collision frequency from coincident radar and Fabry-Perot observations at Millstone Hill, *J. Geophys. Res.*, **102**, 17,267-17,274, (1997).

Buonsanto, M. J., Y.-K. Tung, and D. P. Sipler, Neutral atomic oxygen density from nighttime radar and optical wind measurements at Millstone Hill, *J. Geophys. Res.*, **97**, 8673-8679, (1992).

Burnside, R. G., C. A. Tepley, M. P. Sulzer, T. J. Fuller-Rowell, D. G. Torr, and R. G. Roble, The neutral thermosphere at Arecibo during geomagnetic storms, *J. Geophys. Res.*, **96**, 1289-1301, (1991).

Dalgarno, A, Ambipolar diffusion in the F-region, *J. Atmos. Terr. Phys.*, **26**, 939, (1964).

Drop, D. P., R. R. Meier, J.M Picone, D. J. Strickland, R. J. Cox, A. C. Nicholas, Atomic oxygen in the thermosphere during the July 13, 1982 solar proton event deduced from far ultraviolet images, *J. Geophys. Res.*, **104**, 4267-4278, (1999).

Grossmann, K. U., M. Kaufmann, and E. Gerstner, A global measurement of lower thermosphere atomic oxygen densities, *Geophys. Res. Lett.*, **27**, 1387-1390, (2000).

Hedin, A. E., MSIS-86 thermospheric model, *J. Geophys. Res.*, **92**, 4649-4662, (1987).

Hines, C. O., H. G. Mayr, and C. A. Reddy, On the analysis of geophysical data for an unkown constant, exemplified by the problem of the O+-O collision cross-section, *J. Atmos. Sol. Terr. Phys.*, **59**, 181-189, (1997).

Kita, K., T. Imamura, N. Iwagami, W. H. Marrow, and T. Ogawa, Rocket observation of atomic oxygen and night airglow: Measurement of concentration with an improved resonance fluorescence technique, *Annales Geophysicae*, **14**, 227-237, (1996).

Link, R., and L. L. Cogger, A reexamination of the O I 6300-Å nightglow, *J. Geophys. Res.*, **93**, 9883-9892, (1988).

McDade, I. C., W. E. Sharp, P. G. Richards, and D. G. Torr, On the inversion of O+(2D-2P) 7320 Å twilight airglow observations: A method for recovering both the ionization frequency and the thermospheric oxygen atom densities, *J. Geophys. Res.*, **96**, 259-266, (1991).

Melo, Stella M. L., Hisao Takahashi, B. R. Clemesha, Paulo P. Batista, and D. M. Simonich, Atomic oxygen concentrations from rocket airglow observations in the equatorial region, *J. Atmos. Sol. Terr. Phys.*, **58**, 1935-1942, (1996).

Omidvar, K., R. Menard, M. J. Buonsanto, Emperical determination of the O+O collision frequency, *J. Atmos. Sol. Terr. Phys.*, **60**, 1-12, (1998).

Pesnell, W. D., K. Omidvar, and W. R. Hoegy, Momentum transfer collision frequency of O+-O, *Geophys. Res. Lett.*, **20**, 1343-1346, (1993).

Reddy, C. A., W. R. Hoegy, W. D. Pesnell, H. G. Mayr, and C. O. Hines, Accuracy of O+-O collision cross-section deduced from ionosphere-thermosphere observations, *Geophys. Res. Lett.*, **21**, 2429-2432, (1994).

Salah, J. E, Interim standard for the ion-neutral atomic oxygen collision frequency, *Geophys. Res. Lett.*, **20**, 1543-1546, (1993).

Shepherd, M. G., J. C. McConnell, W. K. Tobiska, G. R. Gladstone, S. Chakrabarti, and G. Schmidtke, Inference of atomic oxygen concentration from rocket remote sensing of optical aurora using horizontal photometers, *J. Geophys. Res.*, **100**, 17,415-17,428, (1995).

Sipler, D. P., M. A. Biondi, and M. E. Zipf, Vertical winds in the midlatitude thermosphere from Fabry-Perot Interferometer measurements, *J. Atmos. Terr. Phys.*, **57**, 621-629, (1995).

Sipler, D. P., M. E. Hagan, M. E. Zipf, and M. A. Biondi, Combined optical and radar wind measurements in the F region over Millstone Hill, *J. Geophys. Res.*, **96**, 21,255-21,262, (1991).

Stallcop, J. R., H. Partridge, and E. Levin, Resonance charge transfer, transport cross section, and collision integrals for $N^+(^3P)$-$N(^4S^0)$ and $O^+(^4S^0)$-$O(^3P)$ interactions, *J. Chem. Phys.*, **95**, 6429-6439, (1991).

Stubbe, P, Frictional forces and collision frequencies between moving ion and neutral gases, *J. Atmos. Terr. Phys.*, **30**, 1965-1985, (1968).

Ward, William E., and Victor I. Fomichev, On the role of atomic oxygen in the dynamics and energy budget of the mesosphere and lower thermosphere, *Geophys. Res. Lett.*, **20**, 1199-1202, (1993).

Table 1. Data Used in this Paper

Date	Number of Data Points	Kp Max 21 00 - 09 00 UT	Date	Number of Data Points	Kp Max 21 00 - 09 00 UT
Aug. 19, 1988	6	2	May 27, 1990	6	7+
Jan. 11, 1989	7	2	Sep. 19, 1990	12	4+
Feb. 8, 1989	12	4	Sep. 21, 1990	14	5+
Mar. 1, 1989	5	4 -	Sep. 12, 1991	20	3 -
Mar. 9, 1989	16	6 -	Oct. 9, 1991	16	4+
Mar. 20, 1989	25	4 -	Mar. 1, 1992	25	5 -
Apr. 13, 1989	13	4	Mar. 2, 1992	11	3+
Aug. 1, 1989	4	2	May 7, 1992	28	3 -
Aug. 9, 1989	10	2 -	Jan. 21, 1993	38	3+
Oct. 5, 1989	44	2+	Jan. 26, 1993	36	5
Oct. 6, 1989	6	3 -	Jan. 27, 1993	35	3
Dec. 29, 1989	52	5	Jan. 28, 1993	11	2
Feb. 20, 1990	52	5	Oct. 14, 1993	3	3+
Feb. 21, 1990	79	5 -	Mar. 12, 1994	8	5+
Feb. 22, 1990	70	3	Mar. 21, 1994	19	5
Mar. 19, 1990	24	6 -	Apr. 15, 1994	16	4 -
Mar. 22, 1990	15	4+	Aug. 7, 1994	5	1+
Mar. 23, 1990	5	4+	Aug. 9, 1994	5	1
Mar. 29, 1990	26	4+	Aug. 16, 1994	4	3+
Apr. 8, 1990	8	3 -	Nov. 10, 1994	3	5 -
Apr. 9, 1990	12	5+	Dec. 3, 1994	35	5 -
Apr. 10, 1990	8	8 -	Jan. 26, 1995	26	1
May 25, 1990	22	4 -	Mar. 3, 1995*	2	3+

*Data from this day was completely rejected as outliers.

Table 2. Standard Deviations and Bias

Set	Data	Standard Deviation	SD/Mean	Bias
A	O	3.1×10^{14}	%27.01	
	D/W	7.1×10^{14}	%52.07	%18.70
B	O	2.7×10^{14}	%30.24	
	D/W	5.6×10^{14}	%50.69	%26.11

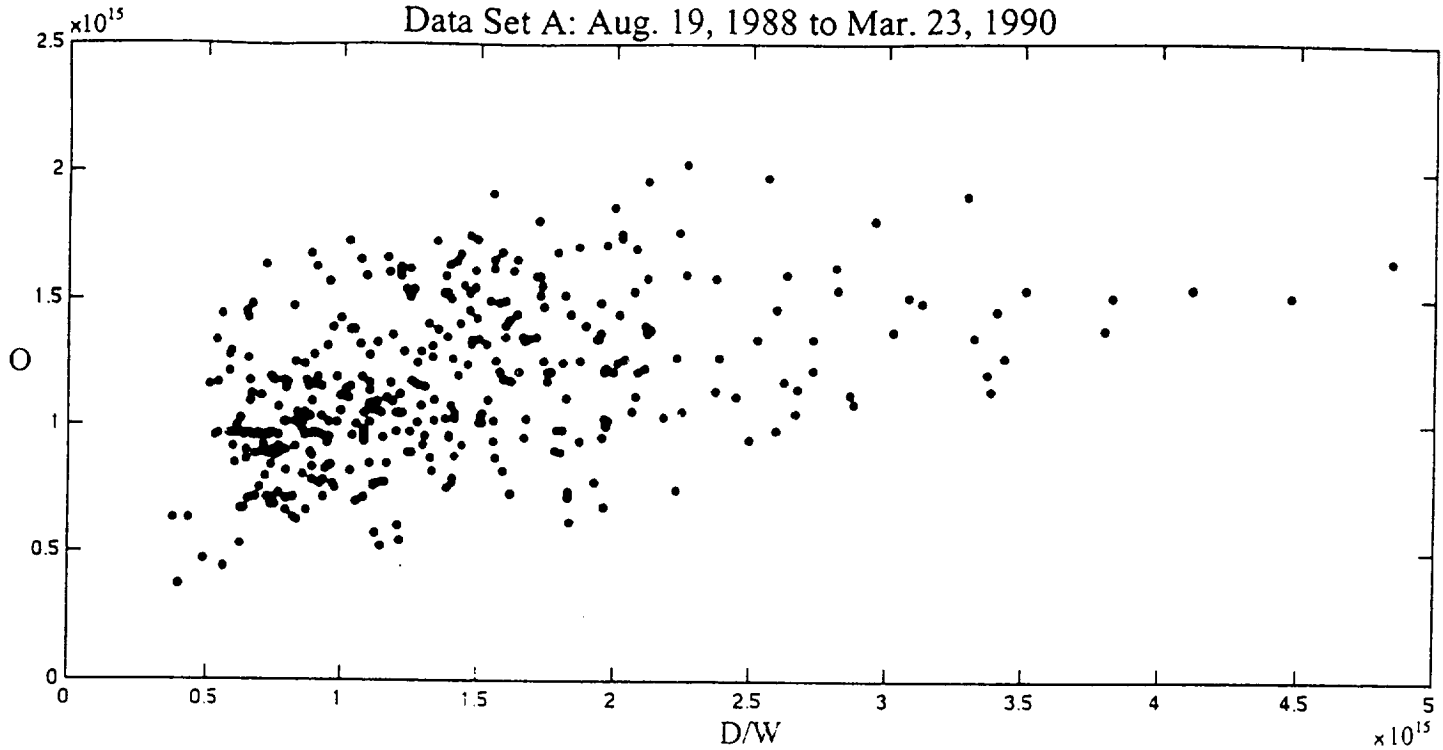

Figure 1: This scatter plot of O versus D/W with outliers removed shows the wide spread of data Set A, although a slight linear relationship is apparent.

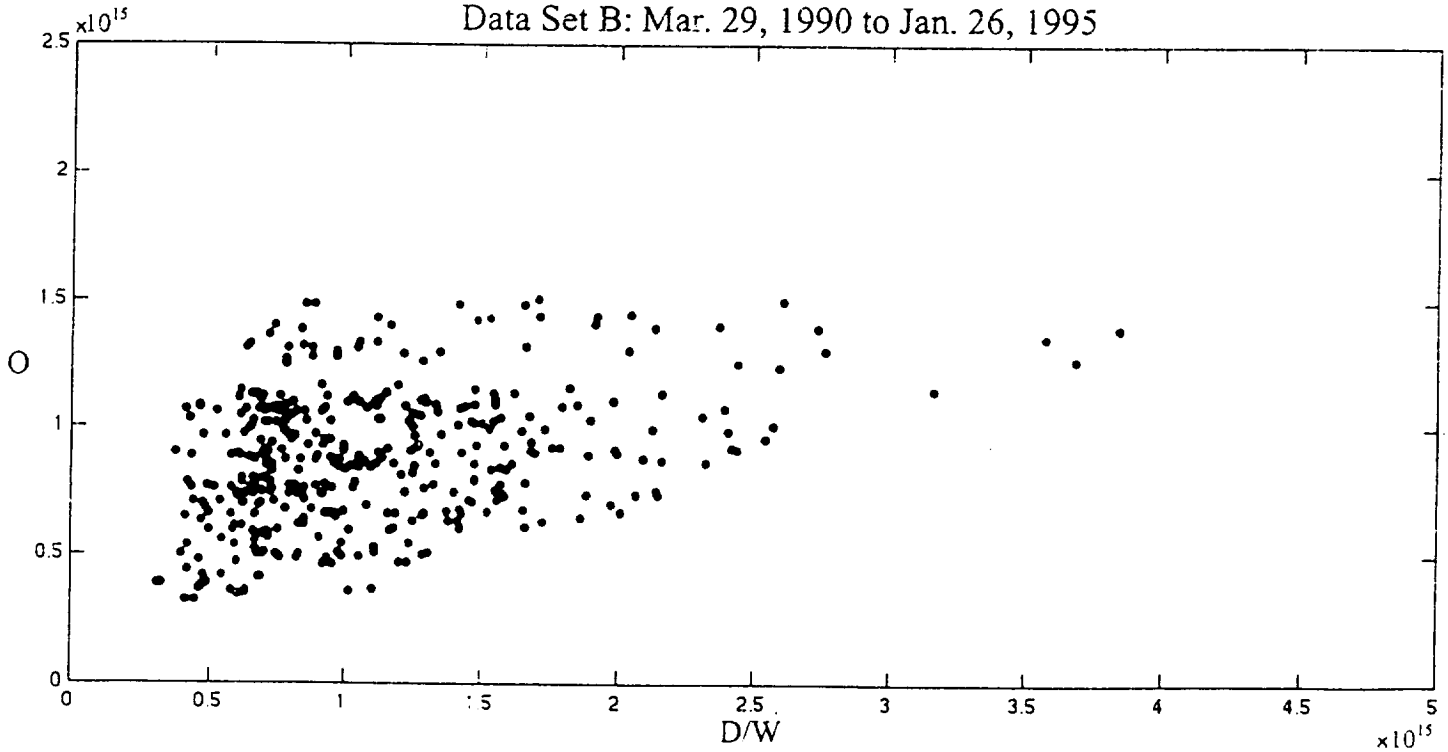

Figure 2: This scatter plot of O versus D/W with outliers removed shows the wide spread of data Set B. A linear relationship is not as visible as Set A.

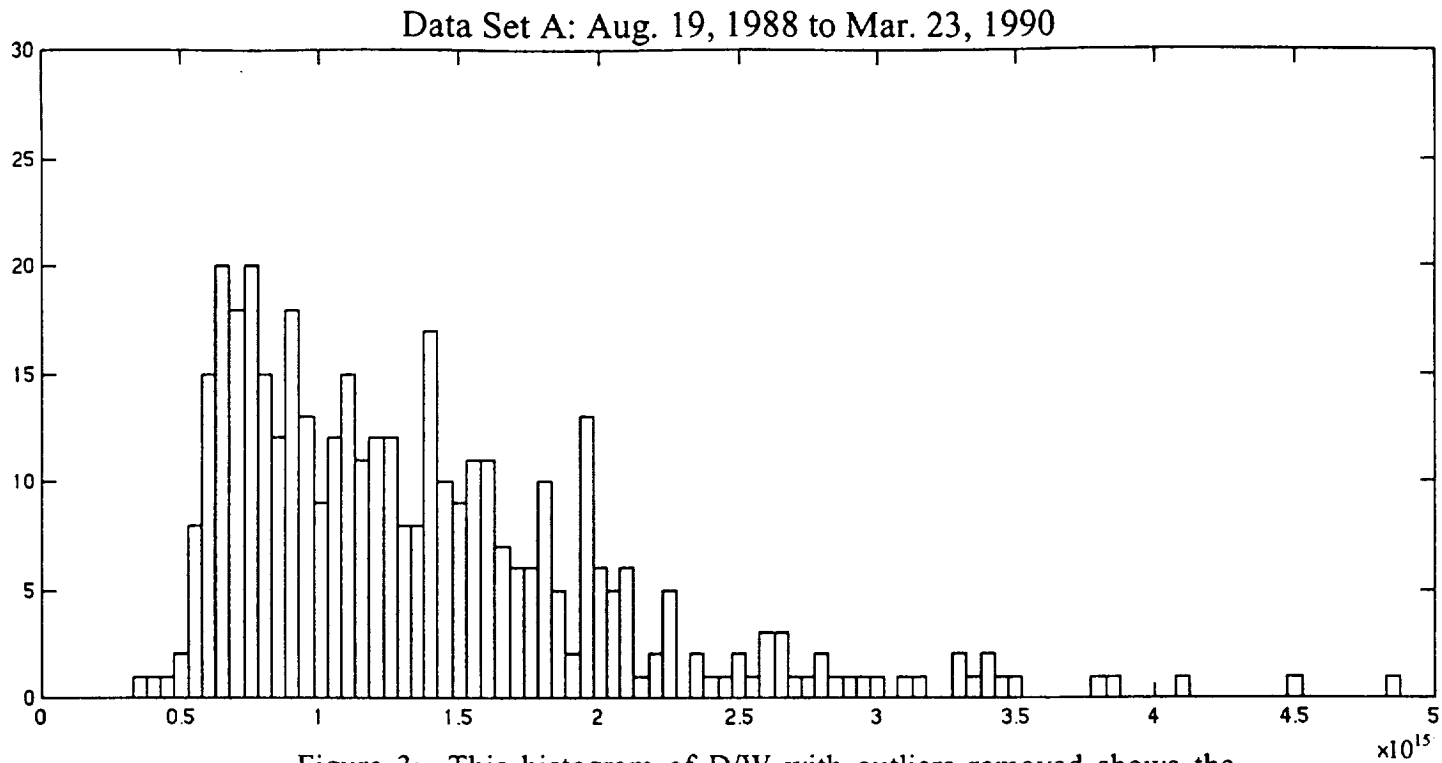

Figure 3: This histogram of D/W with outliers removed shows the distribution of Set A. It approximates a log-normal distribution.

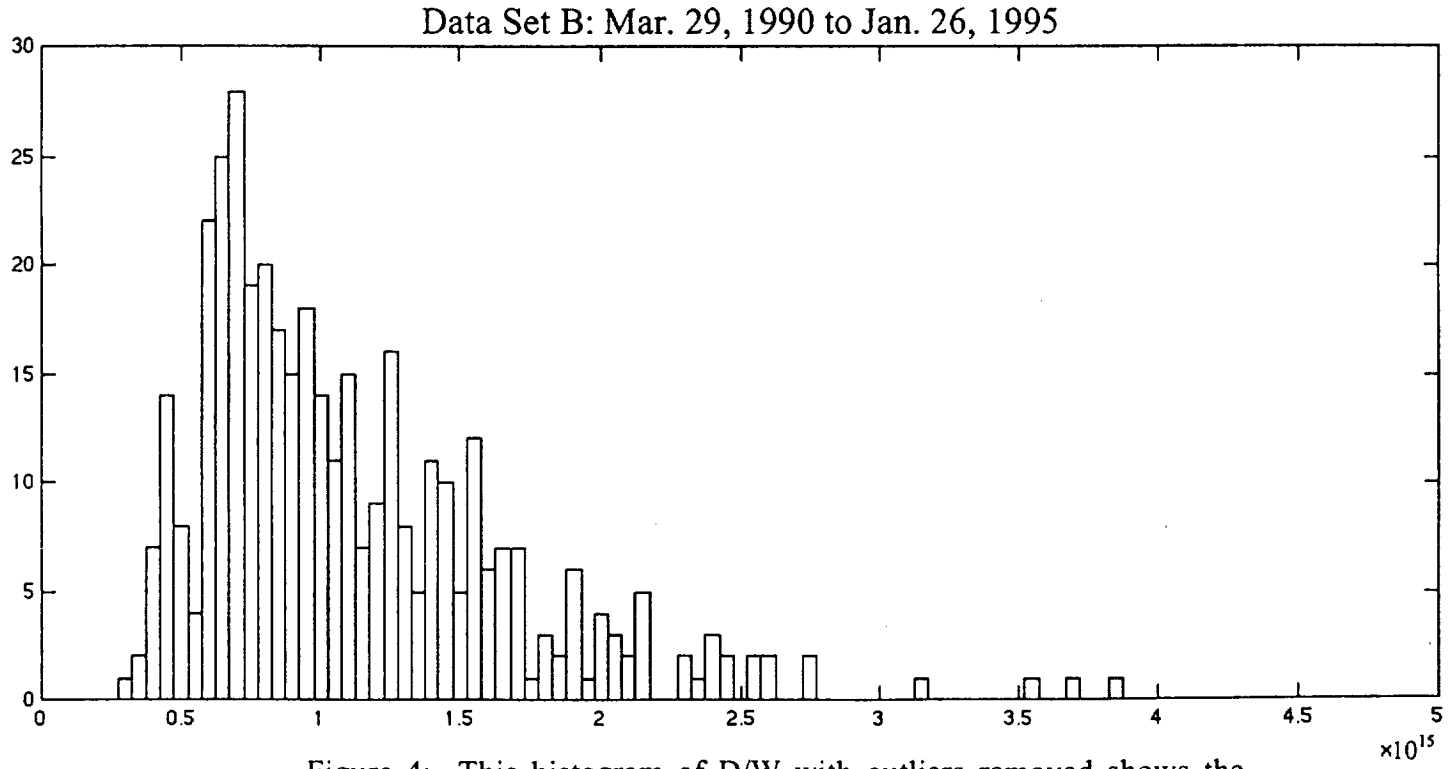

Figure 4: This histogram of D/W with outliers removed shows the distribution of Set B. It approximates a log-normal distribution.

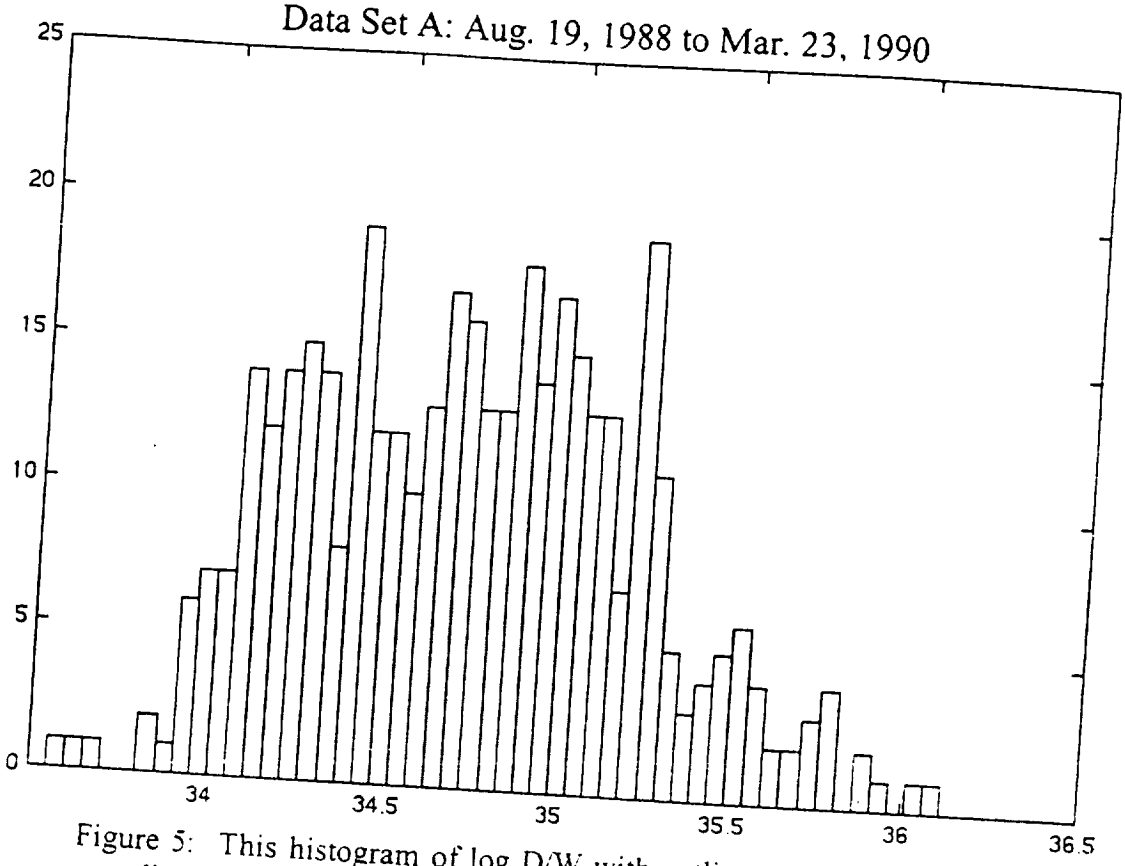

Figure 5: This histogram of log D/W with outliers removed shows the new distribution of Set A. It now approximates a Gaussian distribution.

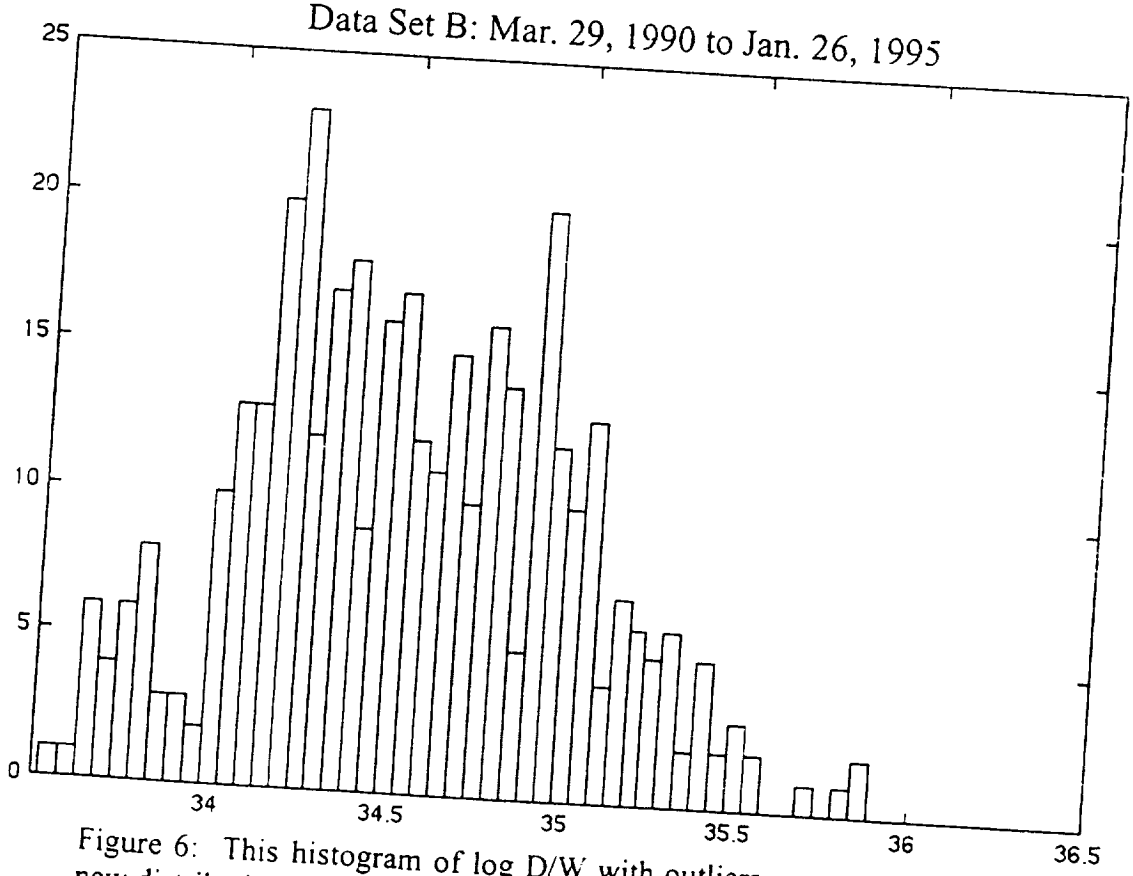

Figure 6: This histogram of log D/W with outliers removed shows the new distribution of Set B. It now approximates a Gaussian distribution.

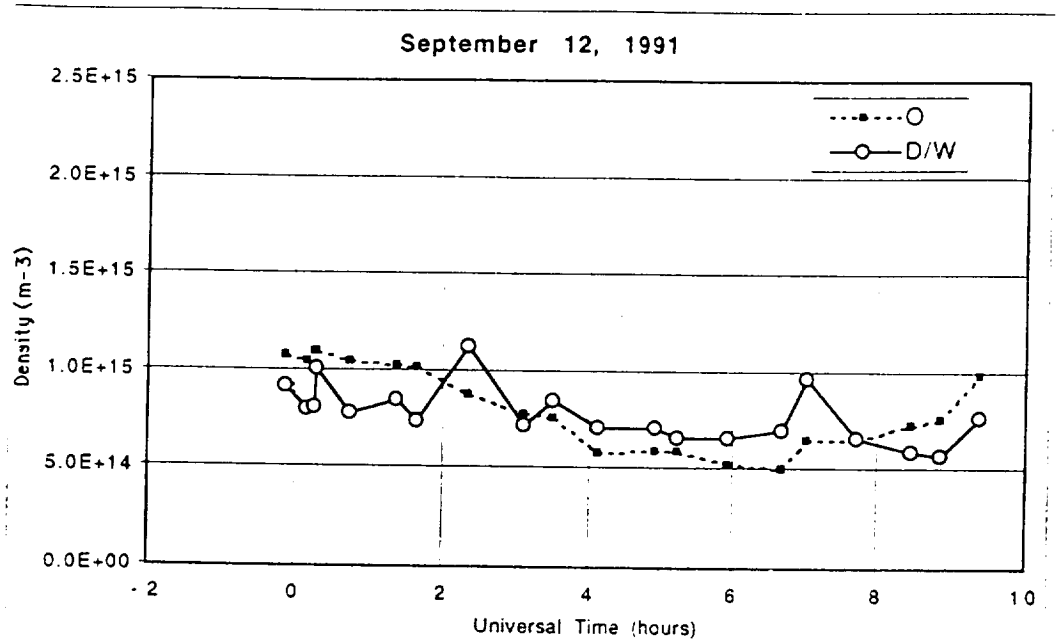

Figure 7: This chart plots the measured D/W and the predicted O versus the time the data was taken. Each O prediction is based upon the estimated altitude the D/W was measured. The measurements vary in altitude, as can be seen by the fluctuations in the O predictions, but generally range no more than 50 km at about a height of 300 km.

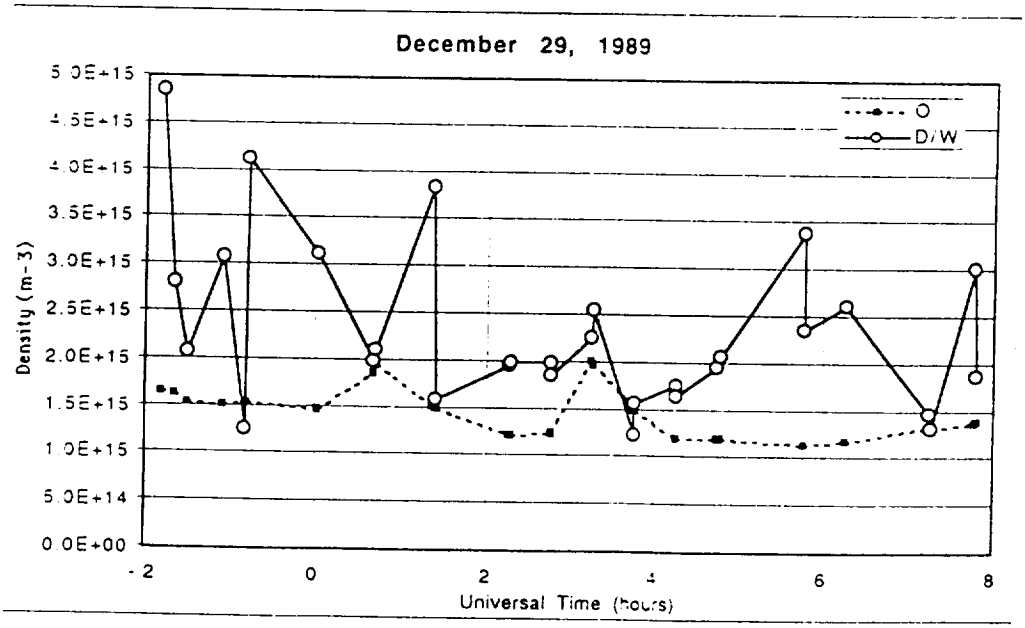

Figure 8: Same as Figure 7. Notice the erratic nature of the measured data.

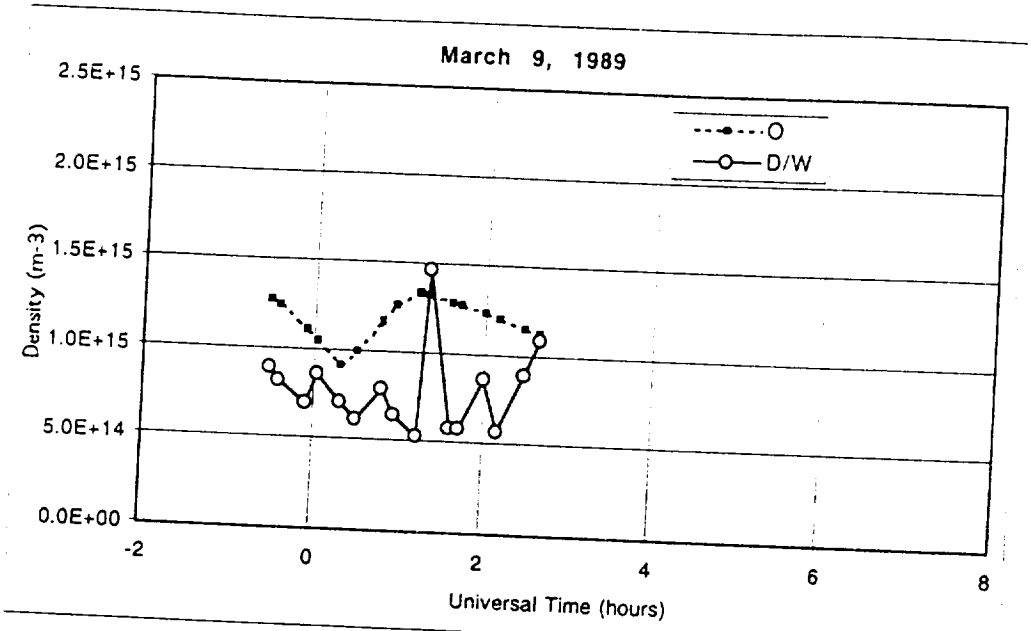

Figure 9: Same as Figure 7. The measured data is consistently lower than predicted.

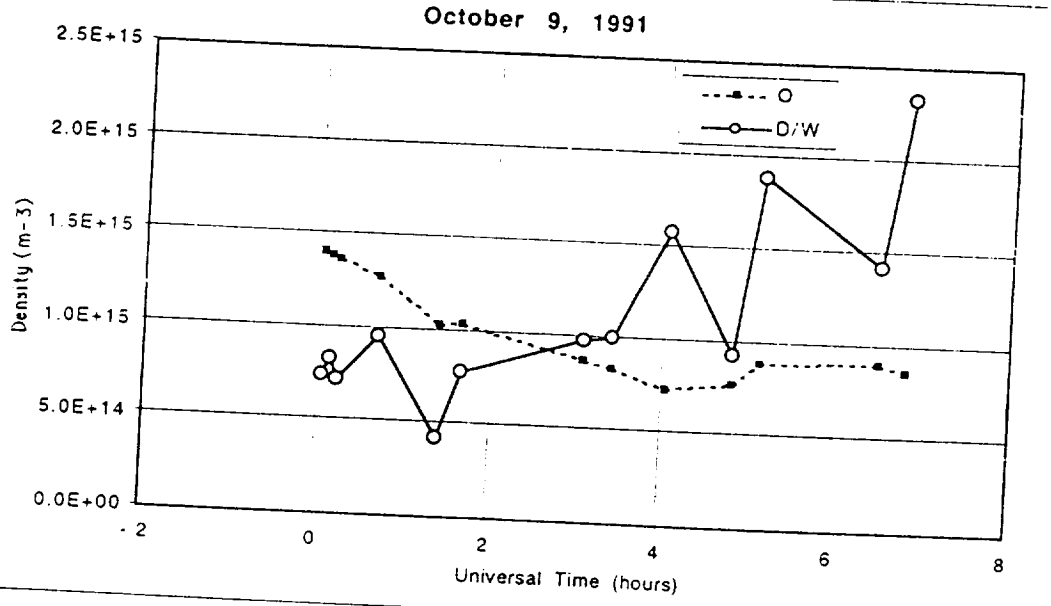

Figure 10: Same as Figure 7. The measured data has an odd upward trend compared to the prediction.

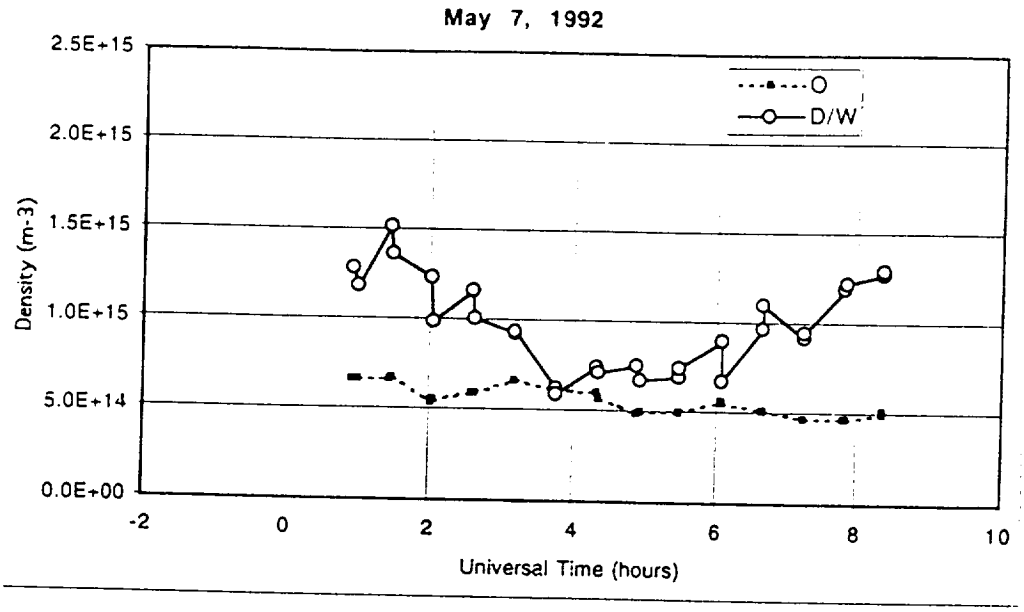

Figure 11: Same as Figure 7. The measured data first exhibits a downward trend, then an upward trend.

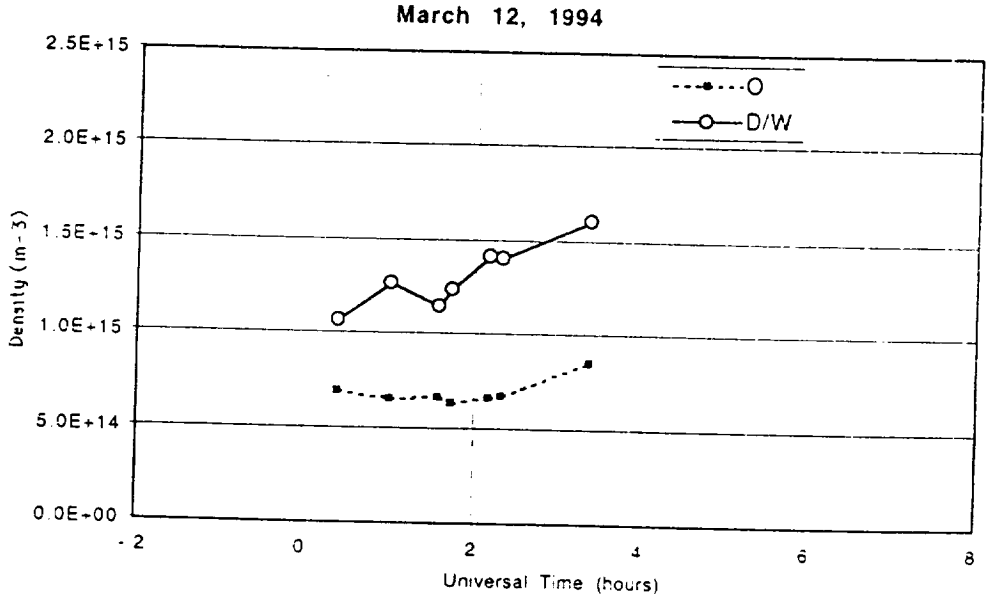

Figure 12: Same as Figure 7. The measured data is substantially larger than predicted.